



Achievement of defect-free and high-properties multilayer copper foils flexible connection by friction stir welding

Zihang Li^{1,2} · Yongfang Deng^{1,2,3} · Jincheng Zeng^{2,4} · Liang Hu^{1,2} · Yutao Zhou^{1,2} · Zherui Qiu⁵

Received: 22 September 2023 / Accepted: 13 December 2023 / Published online: 21 December 2023
© International Institute of Welding 2023

Abstract

The connection of new energy vehicle batteries often involves a copper flexible connection. In this experiment, Friction stir welding (FSW) of multilayer copper foils was proposed for the research of copper flexible connection. It studies the correlation between microhardness profiles, conductivity test data, welding morphology, and process parameters. When the traverse speed (v) is unchanged at 80 mm/min, and the rotation speed (ω) increases from 300,600,900,1200, to 1500 rpm, the copper color of the weld gradually changes from yellow to purple-green. Elongated grains were processed into fine equiaxed and recrystallized grains by FSW. After 900 rpm to 80 mm/min FSW of multilayer copper foils to have a better morphology, the hardness of the (nugget zone) NZ increases by about 23 HV, and the conductivity decreases by about 22 IACS. After FSW, the hardness value is the opposite trend of ω/v changes, and the conductivity value is the similar change trend of ω/v changes in the NZ.

Keywords Multilayer copper foils · Flexible connection · FSW · Conductivity · Hardness

1 Introduction

At present, the flexible connection of copper is a flexible conductive device for the electronics industry, which mainly uses its collapsible and telescopic characteristics to turn on the circuit. It is easy to install, has strong flexibility, and is not limited in the angle of assembly, especially its fast heat dissipation and good electrical conductivity, which are mostly used for the conduction of lithium battery

modules of new energy vehicles [1]. The flexible connection of copper is made by welding multiple layers of copper foil. In the field of multilayer copper foils welding, there are resistance spot welding (RSW), melt inert gas welding (MIG), laser beam welding (LBW), and ultrasonic welding (USW). However, the above process methods are used to weld multilayer copper foils materials, there are mainly high temperatures or vibrations that affect the safety performance of the batteries and the high cost of use, which has become the major problem in the flexible connection of new energy vehicles [2–5].

The invention of FSW provides a new welding technology with wide application prospects. Machniewicz et al. [6] have mentioned that FSW can be used as one method for welding copper metals when braze welding does not yield sufficient weld strength and the use of conventional fusion welding is hampered. Compared with other welding, FSW has less impact on the environment. FSW is a solid-state welding process suitable for the mixing of viscoplastic materials caused by thermomechanical processing. Teimurnezhad et al. [7] have mentioned that FSW copper can be used to obtain a weld without poor welding, and the NZ material is evenly distributed. Wang et al. [8, 9] mentioned that FSW can achieve defect-free joints and the welding temperature is lower relative to conventional welding, and the welding

Recommended for publication by Commission III - Resistance Welding, Solid State Welding, and Allied Joining Process

✉ Yongfang Deng
dengyongfang@jxust.edu.cn

- ¹ Faculty of Materials Metallurgy and Chemistry, Jiangxi University of Science and Technology, Ganzhou 341000, China
- ² Jiangxi Provincial Key Laboratory of Maglev Technology, Ganzhou 341000, China
- ³ National Rare Earth Functional Material Innovation Center, Ganzhou 341000, China
- ⁴ School of Electrical Engineering and Automation, Jiangxi University of Science Technology, Ganzhou 341000, China
- ⁵ Jiangxi Nerin Equipment Co., Ltd, Nanchang 341000, China

material has better microstructure and properties. Pancha et al. [9] mentioned that the FSW process includes welding of the material and plastic deformation but at a temperature below the melting point. FSW tool consisting of a suitable shoulder and a stirring pin is inserted into the welding zone, causing frictional heat and material flow [10]. Due to the plastic deformation of the welded material during the welding process and the heat generated by the friction between the stirring tool and the welded material, the welded material produces metallurgical bonding and mechanical bonding to achieve the purpose of connection [9, 11].

According to the available sources, the existing welding multilayer copper foils flexible connection welding method has the problems of high welding temperature, environmental pollution, and high cost. FSW is thought to be a better welding technique due to its advantages of low processing time, low costs, low welding temperature, and high-quality welding. The experimental study of the fabrication process of multilayer copper foil flexible connection using the FSW process and the study of process parameters have not been done. Due to the application of the subject, in this research, the microstructure and properties of multilayer copper foils using the FSW process were studied experimentally. Especially compared the welding morphology and grain size of the copper base metal (BM) and NZ with different rotational speeds using optical microscope (OM) and electron back-scattered diffraction (EBSD). Joints were analyzed by microhardness Instruments and an eddy current conductivity meter. In this experiment, it is explained that micro hardness profiles through the weld, and conductivity test data are

related to the welding morphology and grain size. The most suitable welding parameters are 900 rpm to 80 mm/min.

2 Experiment

2.1 Materials and methods

As shown in Table 1, the welding material adopts the commercial copper foil material grade TU1 with a density of 8 g/cm^3 and a melting point of 1083°C . It has very low oxygen and impurity content, high purity, strong electrical conductivity, strong thermal conductivity, strong ductility, low air permeability, strong processing performance, strong corrosion resistance, and strong cold resistance. The special properties are mainly used for various wires. The specifications of $80 \text{ mm} \times 60 \text{ mm} \times 0.1 \text{ mm}$ copper foils were used to weld 30 pieces of total thickness of 3 mm for each experiment. Figure 1 shows the application and component pictures of copper foil flexible connection batteries.

In this experiment, HT-JM16 \times 23/2 small FSW equipment was prepared by Aerospace Engineering Equipment (Suzhou) Co. Ltd. The stirring tool uses H13 steel as the processing raw material. Before the experiment, the copper foils used in the experiment were treated with acetone solution to remove oil stains, and then the acetone solution on the surface of the welded workpiece was removed and dried with alcohol. The sample was treated to improve the welding quality and facilitate an effective analysis of the experimental results.

Table 1 Chemical composition of copper foils TU1 (wt. %)

Material	Cu + Ag	P	Bi	Sb	As	Fe	Ni
Copper foils TU1	99.97	0.002	0.001	0.002	0.002	0.004	0.002

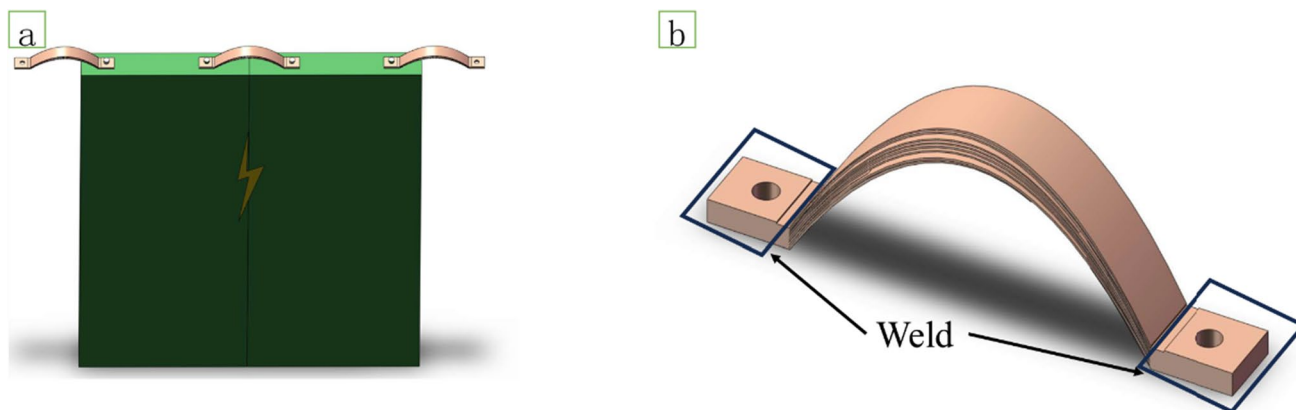


Fig. 1 a Battery module, b copper flexible connection component

As shown in Fig. 2, the metallographic samples were prepared according to the standard metallographic procedure, and the samples were polished with 600 #, 800 #, 1500 #, and 2000 # sandpaper in turn. Copper metallographic etching solution was a mixture of 3 mL HNO₃ and 7 mL C₂H₅O, and it was used for etching for 20~60 s. The microstructure of the weld was observed by OM. Different welding parameters are used to analyze and detect the most suitable process parameters for welding multilayer copper foils. After sanding with sandpaper, the experiment used electrolytic polishing to prepare EBSD samples. The polishing solution was a mixture of 30 mL alcohol and 70 mL phosphoric acid, with a voltage of 20 V, a current of 1 A, and the polishing time was 2 min. The microstructure of the weld was observed by EBSD. EBSD data collection was conducted at step sizes of 0.2 μm, operated at 20 keV. The results from the EBSD were analyzed using Channel 5 software. Different welding parameters are used to analyze and detect the most suitable process parameters for welding multilayer copper foils.

The microhardness of the weld cross-section at TD and ND direction was measured by VH-800 microhardness in Fig. 2c. The interval was 0.5 mm, the loading was 2 N, and the holding time was 10 se. Under different welding parameters, the weld P1 points, and BM were detected by an eddy current conductivity meter. Table 2 selects, in the

Table 2 In this experiment, the Main welding parameters of FSW and the total thickness of copper foils

Sampleno	Tool rotation speed (rpm)	Feed rate (mm/min)	Plunge depth (mm)	Total foils thickness (mm)
1	300	80	0.1	30×0.1
2	600	80	0.1	30×0.1
3	900	80	0.1	30×0.1
4	1200	80	0.1	30×0.1
5	1500	80	0.1	30×0.1

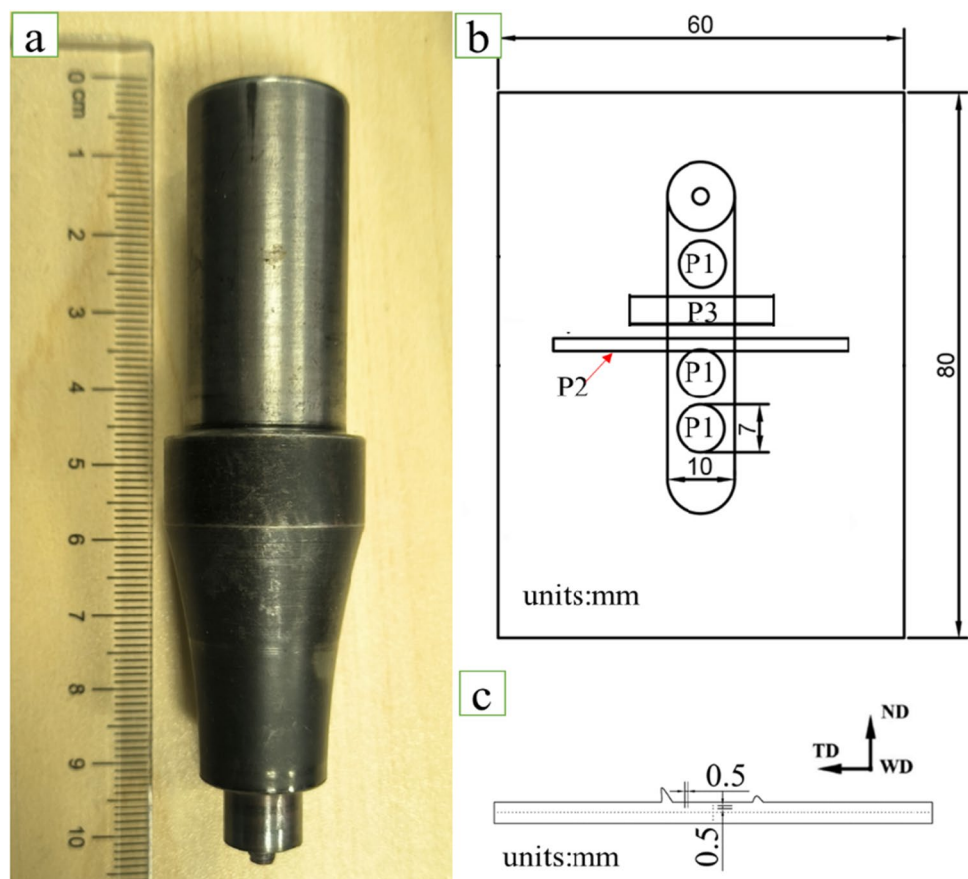
experiment, the welding parameters of FSW and the thickness of copper foils were selected. The above detection temperatures are carried out at room temperature.

3 Results and discussion

3.1 Macroscopic morphology analysis of weld under different welding parameters

In the welding process, the v , ω , and the pressure of the stirring tool have a significant influence on the amount of welding heat input and material flow. The amount of heat input

Fig. 2 a Threaded tool used in the experiment; b welded specimens were taken of the conductivity test specimen prototype P1, EBSD samples P2, and hardness specimen long body P3; c hardness test specimen. Transverse direction (TD), normal direction (ND), and weld direction (WD)



and material flow affects the formation of welding defects such as grooves and flash in the weld. Therefore, the process parameters of stirring in the welding process are the key to controlling the welding quality. The ω and v are one of the most important welding process parameters because these are two parameters determine the size of the welding heat input. Ghosh et al. [12] mentioned that the ω is proportional to the heat input, and the v is inversely proportional to the heat input (Q). The larger the ω/v , the higher the Q . The order of the amount of heat input during welding is as follows: Q (300 rpm to 80 mm/min) < Q (600 rpm to 80 mm/min) < Q (900 rpm to 80 mm/min) < Q (1200 rpm to 80 mm/min) < Q (1500 rpm to 80 mm/min). In this experiment, only the ω is changed and other parameters do not change. Xie

et al. [13] mentioned that with the increase in ω , the heat increases, and the stress zone and strain zone of the welding part also change, which indicates that the FSW welding effect has a great relationship with ω and v of stirring tool. Therefore, optimizing these two process parameters is an indispensable way to obtain better welding materials.

At 300 rpm-80 mm/min, the lack of heat produces severe Grooves that cannot be welded, as shown in Fig. 3a. Mehta et al. [14, 15] mentioned that the heat generated by the interaction between the shoulder of the stirring tool and the material can not completely soften the material, resulting in poor material fluidity, the material cannot be effectively backfilled, and the lower copper foils cannot be welded when the heat is insufficient. Figure 4a illustrates the lack of fusion and

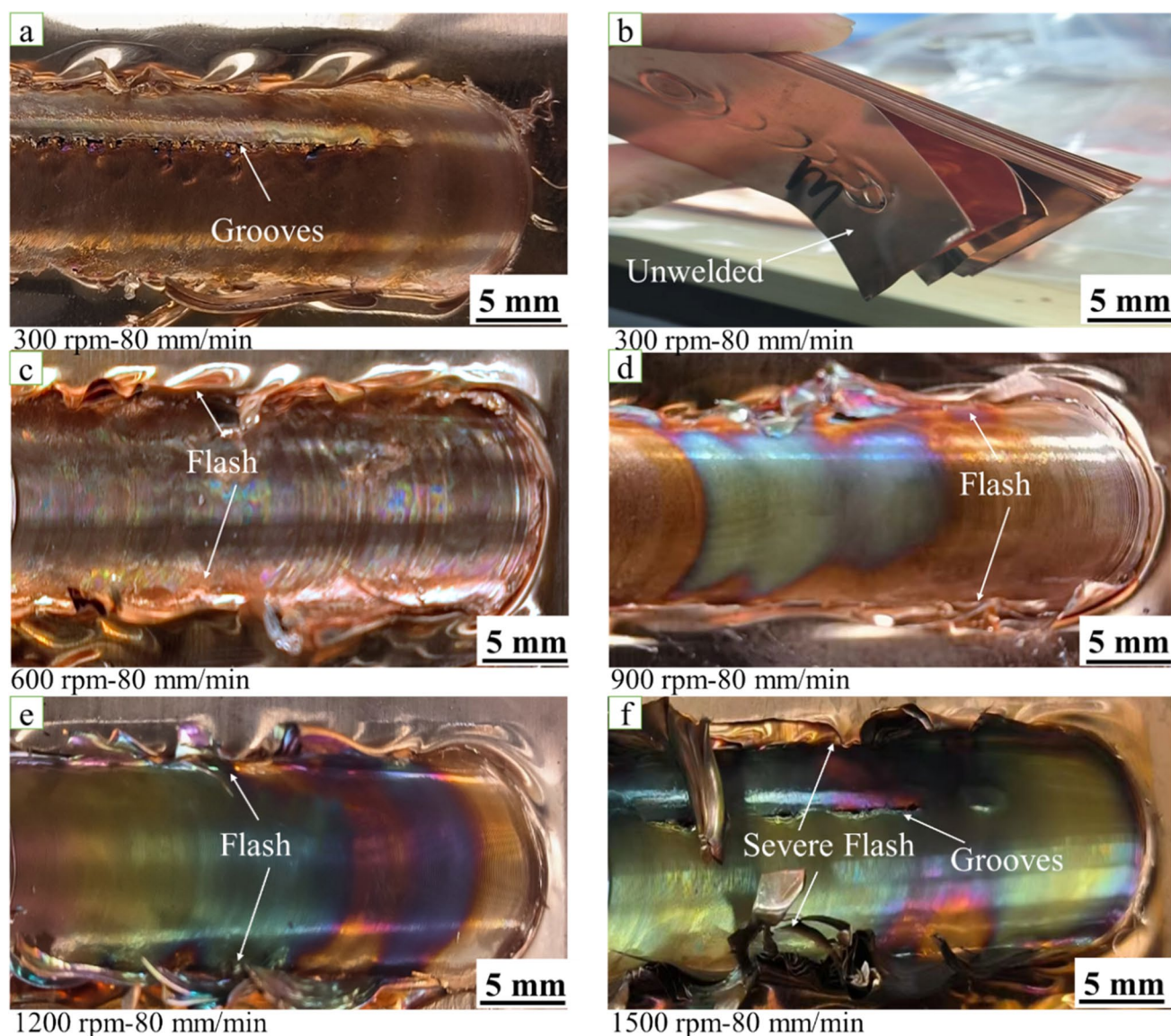
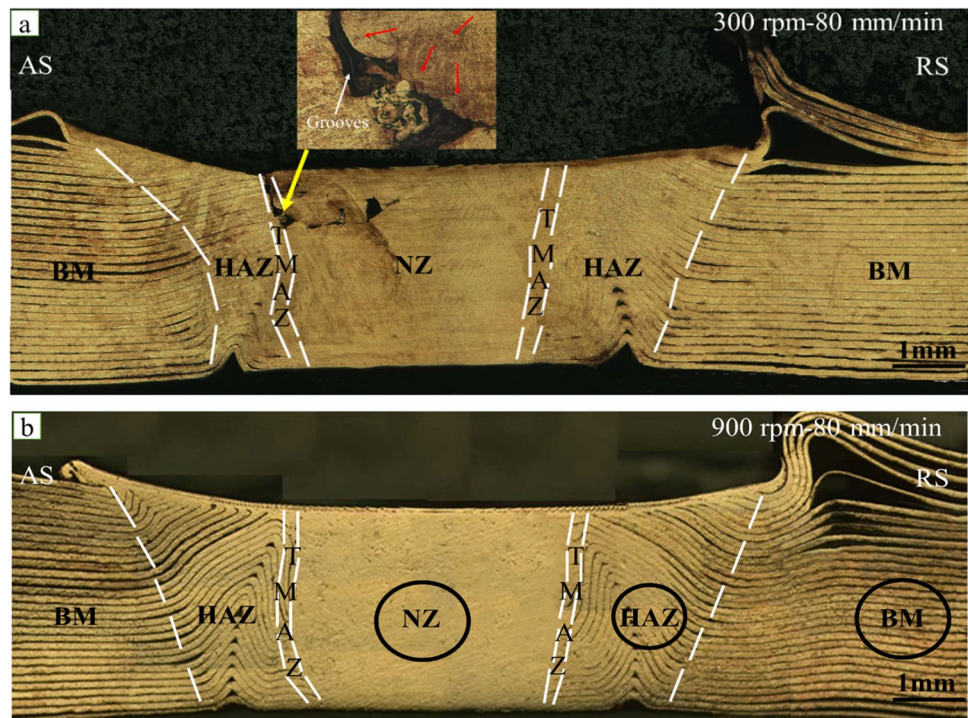


Fig. 3 Welding effect under different welding parameters: **a** grooves; **b** bottom not welded; **c**, **d**, **e** welding morphology is good; **f** grooves and severe flash

Fig. 4 The transverse cross-section of the welds



incomplete penetration on AS. From Fig. 3c, d, e, 600 rpm, 900 rpm, 1200 rpm seam surfaces have a small amount of flash, and it does not affect NZ performance. The wavy flash appears on the outer edge of NZ, and the flash of RS is more severe than the flash of AS, as shown in Fig. 3. Hasan et al. [16] also mentioned that flash is due to the energy accumulated by the upper layers of copper foil in the FSW process is too large, and the metal around the tool shoulder is seriously softened, so that this part of the metal does not rotate around the tool shoulder, and the tool shoulder pushes the material to both sides of the weld in the FSW process. In the FSW process, other parameters remain unchanged, the greater the rotational speed, the greater the force on the upper copper foil and the more heat generated, which will form a large number of flash affecting the performance of NZ. When the ω of the stirring tool is 1500 rpm and the v is 80 mm/min, due to the high heat and high ω , the material is brought to the retreating side (RS) to form a severe flash, thus lacking the material to fill the advancing side (AS) to form severe grooves, and the surface of the NZ is seriously discolored, as shown in Fig. 3f. When the value of ω/v is bigger, the friction between the stirring tool and the material and the extrusion of the material produce too much heat during the welding process, which leads to the liquefaction of some materials in the NZ, and the liquefied metal is squeezed out of the weld surface by the force of the stirring tool, and finally, serious defects such as flash and grooves are formed on both sides of the weld [13]. As shown in Fig. 3, the v remains unchanged, with the increase of the rotational speed, the color of the

weld surface also changes, gradually changing from yellow to purple-green. This is due to the change of copper color caused by high temperature. It is verified by this experiment that the welding quality is the best when the v is 900 rpm and the traveling speed is 80 mm/min.

Figure 4 shows the groove, whereas the groove causes the separation of NZ and thermo-mechanically affected zone (TMAZ), and shows that the end of the crack penetrates NZ (yellow arrow grooves is the enlarged shown in Fig. 4a). Mehta et al. [14] is believed that the material softened rotated from the AS to the RS, and then it back-filled to the AS in FSW process in Fig. 4a red arrow. Under the welding parameters of 300 rpm to 80 mm/min, due to low FSW temperature, no joint is fulfilled between TMAZ and NZ in Fig. 4a. Because the groove greatly affects the material properties, the welding parameters of 300 rpm to 80 mm/min and 1500 rpm to 80 mm/min are not taken in this experiment. There is no obvious volume change of multilayer copper foils after welding with appropriate parameters, and there is no poor welding in the NZ, indicating that FSW can achieve high-quality products by welding multilayer copper foils in Fig. 4b. Table 2 selects in this experiment; the welding parameters of FSW and the thickness of copper foils were selected. From Fig. 4b, the most suitable welding parameters of this experiment are 900 rpm to 80 mm/min. Figure 4b shows EBSD measurement regions (black oval).

Figure 5a shows the horizontal sectional map of the welding material in the radial direction under the welding

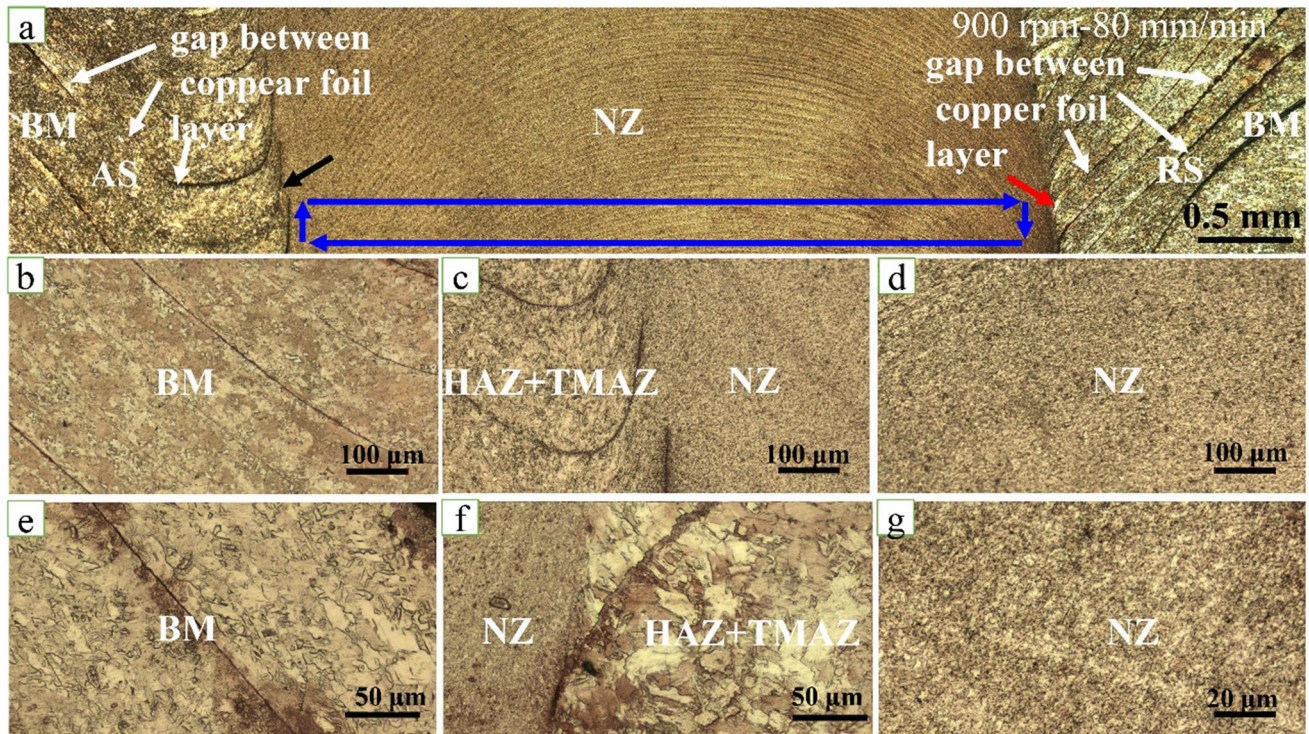


Fig. 5 Under the optimal welding morphology parameters (900 rpm to 80 mm/min), **a** the WD sectional map of the welding material; **b, c, d** BM, thermo-mechanically affected zone (TMAZ)+TMAZ, NZ at the AS; **c, d, e, f, g** BM, HAZ+TMAZ, NZ at the RS

parameters of 900 rpm to 80 mm/min. The onion ring structure can be seen in the NZ. The material near the NZ on the RS of the welding is driven forward by the stirring tool (black arrow), and the material near the NZ on the RS of the welding is driven back by the stirring tool (red arrow). The blue arrow shows that when the plastic metal of the FSW weld flows fully, the material mainly flows from AS to RS, and accumulates layer by layer on the RS, finally forming the weld in Fig. 5. In the BM, we can see the gap between the copper foils layer in Fig. 5. From the BM to the NZ, the color of the gap between the copper foils layer gradually becomes lighter until there is no, indicating that the welding is completed in Fig. 5a, c, and f. During the FSW process, which culminates in the final equiaxial recrystallization of fine grain, the copper in the NZ undergoes continuous dynamic recrystallization due to continuous shearing of the material by the stirring tool in Fig. 5d and g.

3.2 Microstructure of welding zone under different rotational speed

From Fig. 6, the material of multilayer copper foils is refined by FSW, the area-weighted mean grain size in BM is 7.62 μm , the area-weighted mean grain size in NZ-900 rpm is 1.64 μm , and the material in NZ is obviously refined. When the welding parameters are 900 rpm to 80 mm/min,

the grain size of HAZ is the largest in the whole region, which is 8.94 μm . The area-weighted mean grain size in the NZ increased from 1.3 μm , 1.64 μm , and 2.05 μm as the ω increased from 600 rpm, 900 rpm, and 1200 rpm. This is due to the higher heat input (high ω/v) during FSW processing, thus achieving the annealing of the dynamically recrystallized processed structure in NZ. It may be deduced that FSW is favorable to refining the grains of the NZ. The material in the NZ undergoes plastic deformation at high temperatures and strain rates due to the translational and rotational motion of the threaded stirring tool. During the process, which culminates in the final equiaxial recrystallization of fine grain, the copper in the NZ undergoes continuous dynamic recrystallization (CDRX) due to continuous shearing of the material by the stirring tool. Variation in grain refinement in NZ could be due to multiple reasons: variation in (1) grain size of BM, (2) stick-slip coefficient between the stirring tool and copper workpieces, (3) coefficient of friction between the stirring tool and copper workpieces, (4) weld parameter.

3.3 Analysis of hardness test results under different welding parameters

Microhardness is a macroscopic manifestation of the degree of material strengthening in each zone of the welding site. Within a certain range by Hall–Petch relation [17, 18]:

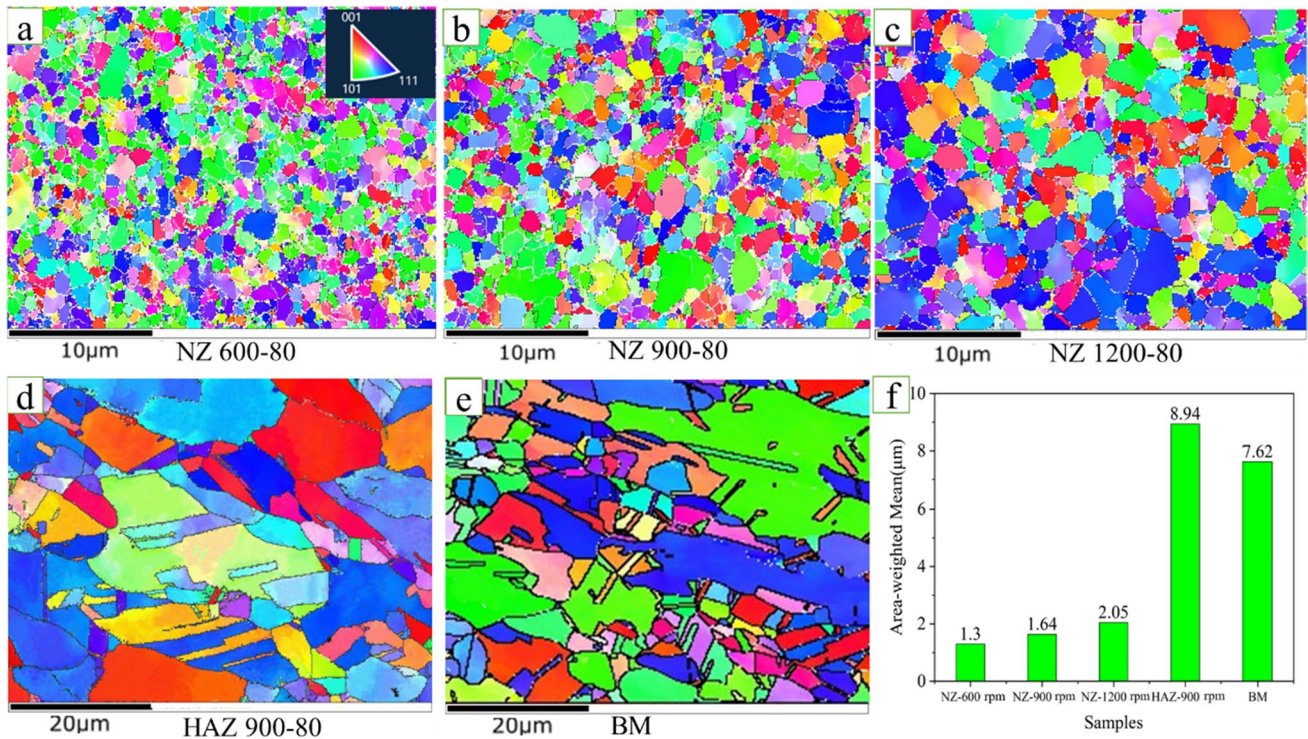


Fig. 6 Shows the EBSD image: **a, b, c** grains in the microstructure of NZ under different welding parameters (rpm-mm/min); **d** grains in the microstructure of HAZ; **e** grains in the microstructure of BM; **f**

the area-weighted mean grain size histograms of NZ, HAZ, and BM under different welding parameters are shown

$$\sigma_{H_p} = \sigma_0 + kd^{-1/2} \tag{1}$$

In the relationship Eq. 1, σ_{H_p} refers to the increase of strength caused by grain boundary effect, σ_0 lattice friction, k is a constant, and d represents the grain size. Within a certain range, it can be seen intuitively from the formula that reducing the grain size can improve the strength without changing the material composition. FSW multilayer copper foils have such fine grain strengthening effect. The order of NZ, HAZ, and BM grain size after welding is as follows: d (NZ-600 rpm to 80 mm/min) < d (NZ-900 rpm to 80 mm/min) < d (NZ-1200 rpm to 80 mm/min) < d (BM) < d (HAZ-900 rpm to 80 mm/min). From Fig. 7, it can be seen that the microhardness of the welding area in the TD is basically a W-shaped distribution. In other words, from the microstructure of the TMAZ to the BM, the microhardness increases significantly, from the NZ to the TMAZ, the microhardness decreases, and the NZ is higher than the BM. It can be seen from Fig. 7 that the microhardness at the centric position of the welding NZ is the highest, up to 110 HV ~ 120 HV. The microhardness of the part of the HAZ is the worst, which is due to the growth grain size in the HAZ under the thermal cycle caused by the FSW processing, resulting in a decrease in the mechanical properties of the area [18, 19]. In

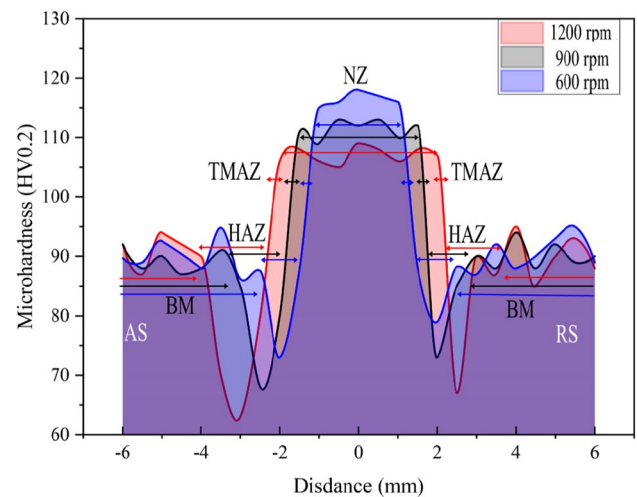


Fig. 7 Hardness distribution in the TD of welding materials under different welding parameters

summary, the microhardness of the HAZ is the worst, which is the lowest hardness of the overall material, and the part of the NZ is where the microhardness is highest. The above trends corresponded well to the area-weighted mean grain size observed in the respective zones of the joint. Thus, the higher hardness in the 900 rpm to 80 mm/min NZ than in

HAZ and BM was related to smaller grain size which was 1.64 μm for NZ, 8.94 μm for HAZ, and 7.62 μm for BM. While for the multilayer copper foils with FSW treatment, the NZ strength is increased, due to fine grain strengthening.

As shown in Fig. 7, the microhardness of RS of the HAZ is obviously higher than that of the AS in the welding direction in processing. Hwang et al. [19–21] concluded that because the temperature of the RS welding is lower than that of the AS, the AS has more heat to HAZ to crystal grain growth, resulting in a lower hardness of the RS after welding relative to the AS of the welding. When the ω is 600 rpm and the speed is 80 mm/min, the heat generated during the stirring welding process is less, and the material softening and plastic deformation are poor, resulting in little change in hardness, but the microhardness of the transition position between the HAZ and the TMAZ is also affected by temperature [21, 22]. When the ω is 1200 rpm and the speed is 80 mm/min, the heat generated during the FSW welding process is too much, resulting in a relatively large decrease in the microhardness of the TMAZ and the HAZ [23]. When the ω is 900 rpm and the speed is 80 mm/min, the HAZ of maximum hardness is 113 HV and the minimum is 73 HV. The grains in the NZ were coarsened to 1.72 μm , 2.49 μm , and 4.16 μm with increasing the rotation rates from 600, and 900 to 1200 rpm, and the hardness decreased gradually. The hardness value is the opposite trend of grain size changes.

The stirring tool with threaded pin guaranteed NZ material flow around the pin, ensuring a defect-free welding FSW process. From Fig. 8, the NZ of the material is uniformly mixed under the action of a threaded stirring tool, and the hardness performance of the material does not change much. Wang et al. [8] have mentioned that the welding temperature in the NZ during FSW was significantly decreased by the

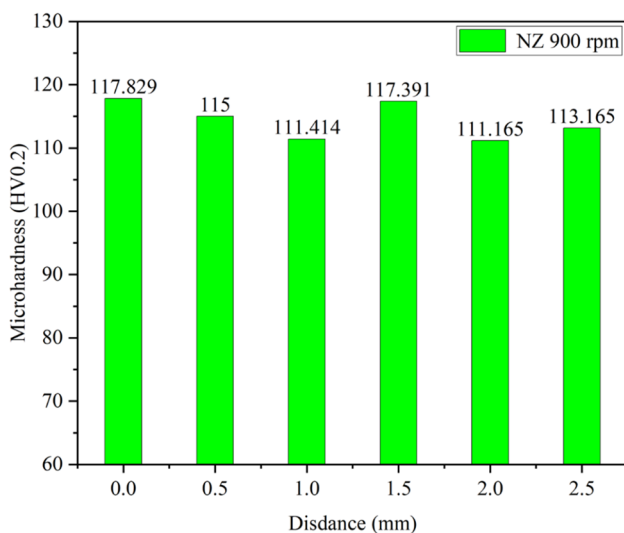


Fig. 8 Under the welding parameters of 900 to 80 mm/min, the ND of the weld center

stirring tool with a threaded pin. Therefore, a stirring tool with a conical threaded pin can be used to increase material hardness under a low heat input.

3.4 Conductivity data analysis under different welding parameters

Abdollah et al. [23] mentioned that copper is mainly used as a conductor, so conductivity is very important for copper. Miyajima et al. [24, 25] mentioned that FSW has the characteristics of plastic deformation after softening the material at high temperature, and then forming fine equiaxed grains through dynamic recrystallization. The conductivity of copper material is well established to depend on the effect of the resistivity of the pure matrix, grain boundary density, impurities, and dislocation density on electron mobility. In the case of the same material, the dislocation density during FSW welding copper is main the factor affecting the conductivity [26, 27]. The main restoration mechanism is CDRX in the NZ, which is the result of a higher dislocation density caused by the FSW process. With the increase of FSW processing ω/v , the dislocation density decreases in NZ, which is due to the main recovery mechanism of CDRX. The smaller the dislocation density, the greater the conductivity of the material, by the law of change in Fig. 9. The electrical conductivity of the BM in the average value is 100.6 IACS, while the electrical conductivity of the 900 rpm to 80 mm/min welding area in the average value is 78.2 IACS, and the electrical conductivity decreases by about 22.5% after FSW in Fig. 9. Although the conductivity of copper decreases a lot after FSW, it is still higher than that of pure aluminum (about 62 IACS) in Fig. 9 yellow line.

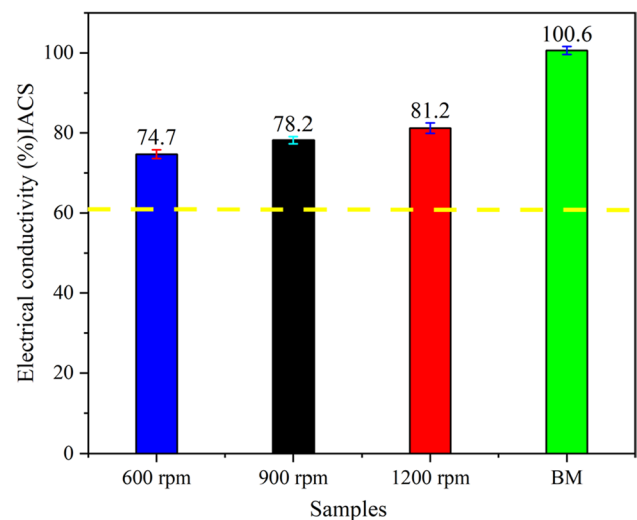


Fig. 9 The conductivity of the welding zone and BM under different welding parameters

As mentioned above, the conductivity of the stirring tool processed materials was found to increase by increasing ω/v . In this way, the increase in conductivity with increasing values of ω/v was affected by dislocation density. Improvement in the electrical conductivity of the processed material is possible to be achieved by increasing the ω/v ratio, but high v is prone to weld defect in Fig. 3f.

4 Conclusion

Based on the flexible connection requirements and characteristics of new energy vehicle battery modules, the experimental analysis and research in this paper show that FSW can perform multilayer copper foils welding. The properties of multilayer copper foils FSW weld were studied by microhardness and conductivity tests as well as microstructure and macrostructure analysis. The constant traverse speeds (80 mm/min) and different ω values (600, 900, and 1200 rpm) were preliminarily selected for producing defect-free welds in terms of their visual. The most suitable welding parameters of this experiment are 900 rpm to 80 mm/min. The relevant conclusions can be summarized as follows:

1. The most suitable welding parameters for FSW of multilayer copper foils are 900 rpm to 80 mm/min. There are no severe flashes, grooves, holes, or other weld defects, which is due to better welding heat. A comprehensive analysis of the material hardness and conductivity value of this parameter is better.
2. The microhardness profiles determined for the cross-section of the weld had a *W*-type shape, and the hardness of NZ is the highest. While for the multilayer copper foils with FSW treatment, the hardness is increased, due to fine grain strengthening. The grains in the NZ were coarsened to 1.72 μm , 2.49 μm , and 4.16 μm with increasing the rotation rates from 600, and 900 to 1200 rpm, and the hardness decreased gradually. The ω/v value is the similar change trend of grain size changes in the NZ and the hardness is the opposite trend of grain size changes.
3. The FSW leads to a decrease in conductivity, which is mainly caused by a large number of dislocations produced in the machining process of the NZ. The conductivity value is a similar trend of ω/v changes.

Author contribution Zihang Li: conceptualization, methodology, validation, formal analysis, investigation, writing—original draft, writing—revise and editing. Yongfang Deng: writing—revise and editing, resources, funding acquisition. Jincheng Zeng: conceptualization, methodology. Liang Hu: investigation. Yutao Zhou: investigation.

Zherui Qiu: investigation. All authors agree to participate in the completion of the manuscript and the publication of the manuscript.

Funding This study was funded by Jiangxi Provincial Natural Science Foundation Project (20212BAB214025); Jiangxi Provincial Department of Education Science and Technology Research Project (GJJ170501); Jiangxi Provincial Department of Education Science and Technology Project (GJJ210882); Ganzhou Science and Technology Plan Project Science and Technology Innovation Talent Program; Ganzhou Science and Technology Plan Project; and Jiangxi University of Science and Technology Ph.D. Foundation Funded Project (JXXJBS16001).

Data availability Data openly available in a public repository.

Declarations

Competing interests The authors declare no competing interests.

Ethical approval The submitted work is original and has not been published elsewhere. The manuscript was not submitted to more than one journal for simultaneous consideration.

References

1. Ye Q, Li A, Fu Q (2021) Effects of preparation methods for Cu foil on the electric-explosion properties. *Propellants Explos Pyrotech* 46:555–562. <https://doi.org/10.1002/prop.202000156>
2. Zhang X, Wei L, Xu G (2019) Connection status research of the resistance spot welding joint based on a rectangular terminal electrode. *Metal* 9:659. <https://doi.org/10.3390/met9060659>
3. Nothdurft S, Seffer O, Hermsdorf J (2022) Investigations on laser beam welding of thin foils of copper and aluminum regarding weld seam quality using different laser beam sources. *J Laser Appl* 34:042–11. <https://doi.org/10.2351/7.0000777>
4. Zhan X, Meng Y, Gu D (2019) A comparative study between pulsed metal inert gas welding and continuous metal inert gas welding on thin Invar alloy. *Proc Inst Mech Eng, Part B: J Eng Manuf* 233:527–538. <https://doi.org/10.1177/0954405417748186>
5. Shin S, Nam S, Yu J (2021) Ultrasonic metal welding of multilayered copper foils to nickel-plated copper sheet in lithium-ion battery cell. *Metals* 11:11–95. <https://doi.org/10.3390/met11081195>
6. Machniewicz T, Nosal P, Korbel A (2020) Effect of FSW traverse speed on mechanical properties of copper plate joints. *Materials* 13:19–37. <https://doi.org/10.3390/ma13081937>
7. Teimurnezhad J, Pashazadeh H, Masumi A (2016) Effect of shoulder plunge depth on the weld morphology, macrograph and microstructure of copper FSW joints (Article). *J Manuf Process* 22:254–259. <https://doi.org/10.1016/j.jmapro.2016.04.001>
8. Wang YD, Zhu SZ, Xie GM (2021) Realising equal-strength welding with good conductivity in Cu–Cr–Zr alloy via friction stir welding. *Sci Technol Weld Joining* 26:448–454. <https://doi.org/10.1080/13621718.2021.1935151>
9. Panchal M, Patel D, Vyas H (2020) Ultra-thin friction stir welding on aluminum alloy. *Mater Today: Proc* 26:2888–2894. <https://doi.org/10.1016/j.matpr.2020.02.597>
10. Guan W, Shen Y, Yan Y (2018) Fabrication of ultra-thin copper foil pressure welding using FSW equipment. *J Mater Process Technol* 251:343–349. <https://doi.org/10.1016/j.jmatprotec.2017.08.022>
11. Gera D, Fu B, Suhuddin UFHR (2021) Microstructure, mechanical and functional properties of refill friction stir spot welds on

- multilayered aluminum foils for battery application. *J Mater Res Technol* 13:2272–2286. <https://doi.org/10.1016/j.jmrt.2021.06.017>
12. Ghosh M, Kumar K, Mishra RS (2011) Friction stir lap welded advanced high strength steels: microstructure and mechanical properties. *Mater Sci Eng Struct Mater: Prop Misrostructure Process* 528:8111–8119. <https://doi.org/10.1016/j.msea.2011.06.087>
 13. Xie G, Cui H, Luo Z (2017) Asymmetric distribution of microstructure and impact toughness in stir zone during friction stir processed a high strength pipeline steel. *Mater Sci Eng, A* 704:401–411. <https://doi.org/10.1016/j.msea.2017.08.008>
 14. Mehta KP, Badheka VJ (2017) Influence of tool pin design on properties of dissimilar copper to aluminum friction stir welding. *Trans Nonferrous Metals Soc China* 27:36–54. [https://doi.org/10.1016/S1003-6326\(17\)60005-0](https://doi.org/10.1016/S1003-6326(17)60005-0)
 15. Pradeep S, Jain VKS, Muthukumaran S (2021) Microstructure and texture evolution during multi-pass friction stir processed AA5083. *Mater Lett* 288:129–382. <https://doi.org/10.1016/j.matlet.2021.129382>
 16. Hasan AF (2019) CFD modelling of friction stir welding (FSW) process of AZ31 magnesium alloy using volume of fluid method. *J Market Res* 8:1819–1827. <https://doi.org/10.1016/j.jmrt.2018.11.016>
 17. Sakthivel T, Mukhopadhyay J (2007) Microstructure and mechanical properties of friction stir welded copper. *J Mater Sci* 42:8126–8129. <https://doi.org/10.1007/s10853-007-1666-y>
 18. Carlton CE, Ferreira PJ (2007) What is behind the inverse Hall-Petch effect in nanocrystalline materials? *Acta Mater* 55:3749–3756. <https://doi.org/10.1016/j.actamat.2007.02.021>
 19. Velichko OV, Ivanov SY, Karkhin VA (2016) Structure and properties of thick-walled joints of alloy 1570S prepared by friction stir weldin. *Met Sci Heat Treat* 58:346–351. <https://doi.org/10.1007/s11041-016-0015-7>
 20. Hwang Y, Fan P, Lin C (2010) Experimental study on friction stir welding of copper metals. *J Mater Process Technol* 210:1667–1672. <https://doi.org/10.1016/j.jmatprotec.2010.05.019>
 21. Naqibi MF, Elyasi M, Aval HJ (2021) Theoretical and experimental studies on fabrication of two-layer aluminum–copper pipe by friction stir additive manufacturing. *Trans Nonferrous Met Soc China* 31:3643–3658. [https://doi.org/10.1016/s1003-6326\(21\)65754-0](https://doi.org/10.1016/s1003-6326(21)65754-0)
 22. Muhammad NA, Wu C (2020) Evaluation of capabilities of ultrasonic vibration on the surface, electrical and mechanical behaviours of aluminium to copper dissimilar friction stir welds. *Int J Mech Sci* 183:105–784. <https://doi.org/10.1016/j.ijmecsci.2020.105784>
 23. Abdollah-Zadeh A, Saeid T, Sazgari B (2008) Microstructural and mechanical properties of friction stir welded aluminum/copper lap joints. *J Alloy Compd* 460:535–538. <https://doi.org/10.1016/j.jallcom.2007.06.009>
 24. Wang YD, Xue P, Liu FC (2023) Influence of processing innovations on joint strength improvements in friction stir welded high strength copper alloys. *Mater Sci Eng, A* 872:144–983. <https://doi.org/10.1016/j.msea.2023.144983>
 25. Miyajima Y, Komatsu SY, Mitsuhashi M (2010) Change in electrical resistivity of commercial purity aluminum severely plastic deformed. *Phil Mag* 90:4475–4488. <https://doi.org/10.1080/14786435.2010.510453>
 26. Leal RM, Galvao I, Loureiro A (2015) Effect of friction stir processing parameters on the microstructural and electrical properties of copper. *Int J Adv Manuf Technol* 80:1655–1663. <https://doi.org/10.1007/s00170-015-7141-z>
 27. Lipińska M, Bazarnik P, Lewandowska M (2016) The influence of severe plastic deformation processes on electrical conductivity of commercially pure aluminium and 5483 aluminium allo. *Arch Civ Mech Eng* 16:717–723. <https://doi.org/10.1016/j.acme.2016.04.013>

Publisher's Note Springer Nature remains neutral with regard to jurisdictional claims in published maps and institutional affiliations.

Springer Nature or its licensor (e.g. a society or other partner) holds exclusive rights to this article under a publishing agreement with the author(s) or other rightsholder(s); author self-archiving of the accepted manuscript version of this article is solely governed by the terms of such publishing agreement and applicable law.